

Excellence in Chemistry Research

Announcing our new flagship journal

- Gold Open Access
- Publishing charges waived
- Preprints welcome
- Edited by active scientists



Meet the Editors of *ChemistryEurope*



Luisa De Cola
Università degli Studi
di Milano Statale, Italy



Ive Hermans
University of
Wisconsin-Madison, USA



Ken Tanaka
Tokyo Institute of
Technology, Japan

Special
Collection

Precision Glycodendrimers for DC-SIGN Targeting

Giulio Goti,^[a] Cinzia Colombo,^[a] Silvia Achilli,^[b] Corinne Vivès,^[b] Michel Thépaut,^[b] Joanna Luczkowiak,^[c] Nuria Labiod,^[c] Rafael Delgado,^[c, d] Franck Fieschi,^{*[b]} and Anna Bernardi^{*[a]}

Dedicated to Professor Cesare Gennari on the occasion of his 70th birthday.

Multivalent ligands of the C-type lectin receptor DC-SIGN have emerged as effective antiadhesive agents against various pathogens. Some years ago, we described a hexavalent DC-SIGN ligand, Polyman-26, designed to bridge two of the four binding sites displayed by the receptor. In this work, we present our efforts to accomplish simultaneous coordination of all four carbohydrate binding sites of DC-SIGN through the synthesis of cross-shaped glycodendrimers. The tailored rigid scaffold allowed multivalent presentation of glycomimetics in a spatially

defined fashion, while providing good water solubility to the constructs. Evaluation of the biological activity by SPR assays revealed strong binding avidity towards DC-SIGN and increased selectivity over langerin. Inhibition of DC-SIGN binding to SARS-CoV-2 spike protein and of DC-SIGN mediated Ebola virus *trans*-infection testifies for the glycodendrimers potential application in infection diseases. The tetravalent platform described here is easily accessible and can be used in modular fashion with different ligands, thus lending itself to multiple applications.

Introduction

Carbohydrate-protein interaction in living systems is an archetype of multivalency, where proteins (called lectins) presenting either multiple carbohydrate recognition domains (CRDs) or an oligomeric structure selectively recognize and bind to specific polyglycosylated targets.^[1] This strategy takes advantage of the mechanisms governing multivalency, *i.e.* chelation, statistical rebinding and receptor clustering, to provide strong binding, while overcoming the intrinsic low affinity of the monovalent glycan ligands for their receptors.^[2–4]

Following the very same approach, the past two decades have seen a prosperous generation of multivalent glycoconju-

gate antagonists able to interfere with such interactions.^[5–9] Altogether, these studies revealed the complexity in designing effective antagonists, whose efficacy is determined by the nature of the ligand displayed, as well as by parameters difficult to predict, such as the architecture of the polyvalent scaffold, the valency, the ligand density, the kind of linker engaged and the flexibility of the construct.^[10]

Lately, we have disclosed structure-based design as a guiding principle in the development of strong polyglycosylated antagonists for Dendritic Cell-Specific Intercellular adhesion molecule-3 (ICAM-3)-Grabbing Non-integrin (DC-SIGN),^[11–14] a tetrameric transmembrane C-type lectin receptor (Figure 1) exploited by pathogens such as HIV, Ebola, Hepatitis C, to invade the host and propagate the infection.^[15,16] While multiple ligand presentation on polyvalent scaffolds is generally the choice to reach high avidity towards DC-SIGN,^[7–9] we showed that scaffold optimization plays a role in achieving high affinity levels with constructs of relatively low valency. Specifically, rigid

[a] Dr. G. Goti, Dr. C. Colombo, Prof. Dr. A. Bernardi
Dipartimento di Chimica
Università degli Studi di Milano
via Golgi 19, 20133, Milano, Italy
E-mail: anna.bernardi@unimi.it

[b] Dr. S. Achilli, Dr. C. Vivès, Dr. M. Thépaut, Prof. Dr. F. Fieschi
Institut de Biologie Structurale
Université Grenoble Alpes, CEA, CNRS
avenue des Martyrs 71, 38000, Grenoble, France
E-mail: franck.fieschi@ibs.fr

[c] Dr. J. Luczkowiak, N. Labiod, Prof. Dr. R. Delgado
Instituto de Investigación Hospital 12 de Octubre
Avenida de Córdoba, 28041, Madrid, Spain

[d] Prof. Dr. R. Delgado
Departamento de Medicina
Universidad Complutense de Madrid
Plaza Ramón y Cajal, 28040, Madrid, Spain

[**] A previous version of this manuscript has been deposited on a preprint server (<https://doi.org/10.26434/chemrxiv.1292221.v1>).

Supporting information for this article is available on the WWW under <https://doi.org/10.1002/ejoc.202200113>

Part of the "DCO-SCI Prize and Medal Winners 2020/2021" Special Collection.

© 2022 The Authors. European Journal of Organic Chemistry published by Wiley-VCH GmbH. This is an open access article under the terms of the Creative Commons Attribution License, which permits use, distribution and reproduction in any medium, provided the original work is properly cited.

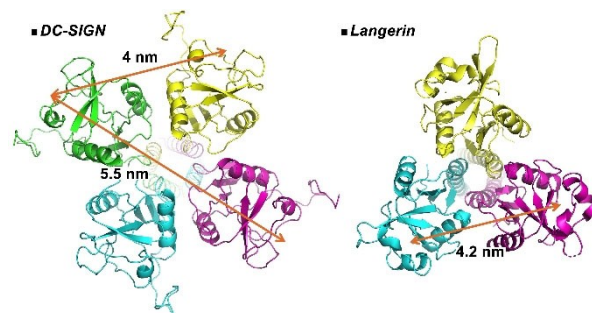


Figure 1. SAXS-derived model of the DC-SIGN ECD tetramer and crystallographic structure of langerin ECD trimer. The four CRDs of DC-SIGN are exposed at the vertexes of a square with a diagonal distance of 5.5 nm.; langerin is characterized by a trefoil structure displaying three CRDs which are spaced by 4.2 nm.

rod-like scaffolds of controlled length were loaded with glycodendrons, giving access to hexavalent constructs (Polyman-31 **PM31** and Polyman-26 **PM26**, depending on the monovalent ligand, Figure 2)^[12,17] able to bridge two contiguous CRDs within the DC-SIGN tetramer, that are separated by ca. 4 nm, or even CRDs at opposite corners of the tetramer, which, on average, are separated by ca. 5.5 nm (Figure 1).^[18] We have shown that these constructs reach nanomolar avidity by combining chelation with statistical rebinding effects due to a high local concentration of monovalent ligands in the proximity of the sugar binding site.^[12,17–19] These dendrimers showed nanomolar activity in the inhibition of DC-SIGN mediated HIV^[12,19] and SARS-CoV-2^[20] infection, in sharp contrast with the low micromolar activity range of less preorganized structures of similar or even higher valency.^[21]

The strong impact of chelation on the inhibition potency led us to consider whether stronger antagonists could be obtained by simultaneous binding of the four CRDs of DC-SIGN extra-cellular domain (ECD). In small-angle X-ray scattering (SAXS) derived models,^[22] they are arranged at the four corners of a square with 4 nm side and diagonals going from 5.2 to 6 nm (Figure 1). Moreover, individual CRDs within the tetramer were described as highly dynamic, suggesting that binding sites topology may be able to adjust to favor higher levels of chelation.^[18] Thus, a modular design, based on a rigid core of appropriate topology and low-valency ligand presentation is expected to provide optimal match.

To test this hypothesis, we targeted the synthesis of cross-shaped glycodendrimers **PM59** and **PM58** (Figure 2). These compounds are characterized by a tetravalent rigid core, composed of two intercrossing rods. The distance between two substituted nitrogen atoms of opposite triazole rings in **PM26,31** (Figure 2) is of 23.5 Å, measured as an average of 1000 poses collected during a molecular dynamics simulation of **PM31**.^[12] This provides a good estimate of the diagonal length

of the rigid core in **PM58,59**. The cross core is then prolonged by four copies of a trivalent glycodendron, resulting in an extended distance over 6 nm between two complexing units.^[12] As monovalent ligands, we selected the pseudo-disaccharide **1** and the corresponding more potent bis-*p*-hydroxymethylenbenzylamide derivative **2**, which we previously reported as effective and selective DC-SIGN antagonists.^[11,23] Ideally, the tailored geometry of the scaffold would confer optimal ligand presentation towards DC-SIGN, while disfavoring binding to C-type lectins characterized by a different spatial arrangement of their CRDs. This concept has been recently exploited to prepare glycosylated antagonists with selectivity for DC-SIGN over langerin and for langerin over ConA.^[24] In particular, a polyproline tetra-helix macrocyclic scaffold adorned with oligomannoside ligands was shown to effectively bind DC-SIGN with K_D in the low nanomolar range and almost 5000 fold selectivity over langerin.^[24a] Selectivity towards DC-SIGN is indeed crucial in order to inhibit its biological functions without interfering with the protective mechanisms provided by other C-type lectins.

Herein, we report the synthesis of compounds **PM58,59** and the evaluation of their interaction with DC-SIGN by Surface Plasmon Resonance (SPR). Selectivity over langerin, a trimeric C-type lectin able to induce virus elimination and clearance in HIV infection,^[25] was also assessed. Moreover, we show that **PM58,59** are effective at preventing DC-SIGN binding to SARS-CoV-2 spike protein and that, at 0.5 μM , they block DC-SIGN mediated trans-infection by Ebola virus.

Results and Discussion

Synthesis of cross-shaped glycodendrimers

For the synthesis of glycodendrimers **PM59** and **PM58**, we identified the tetravalent phenylene-ethynylene core **6** as a key

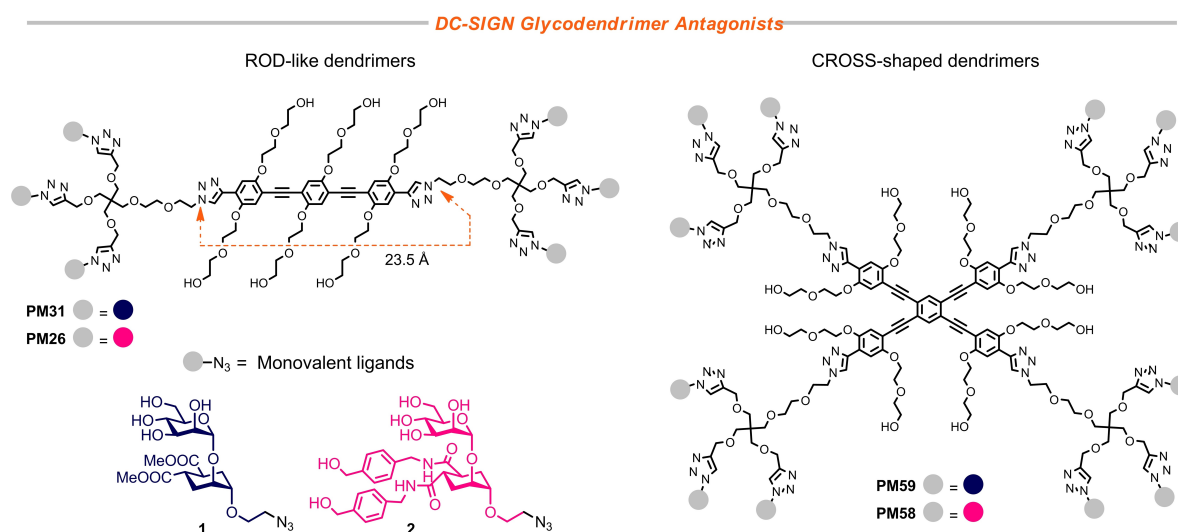


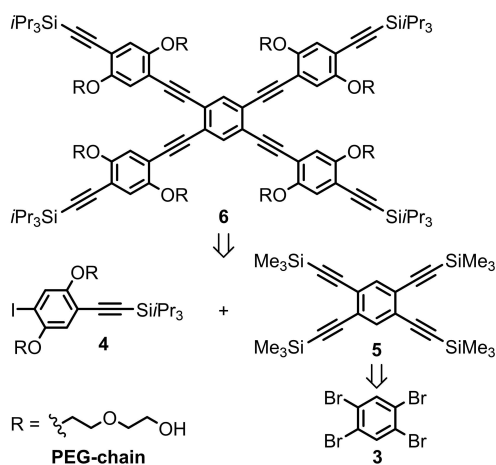
Figure 2. Structures of the previously developed rigid linear glycodendrimers **PM31**, **PM26**^[12] and of the targeted cross-shaped glycodendrimers **PM58,59**. The N–N length of the rigid rod core is indicated and provides a good estimate for the diagonal length of the cross core. Both scaffolds are functionalized with multiple copies of either the pseudo-dimannobioside **1** or with the bis-amido derivative **2**.

intermediate, which enables for late-stage diversification at its four ends through copper catalyzed alkyne azide cycloaddition (CuAAC) (Scheme 1). From a retrosynthetic point of view, the central core **6** can originate from the iodide synthon **4**^[26] and the protected tetraalkynylbenzene unit **5**, whose synthesis has been reported starting from 1,2,4,5-tetrabromobenzene **3**.^[27]

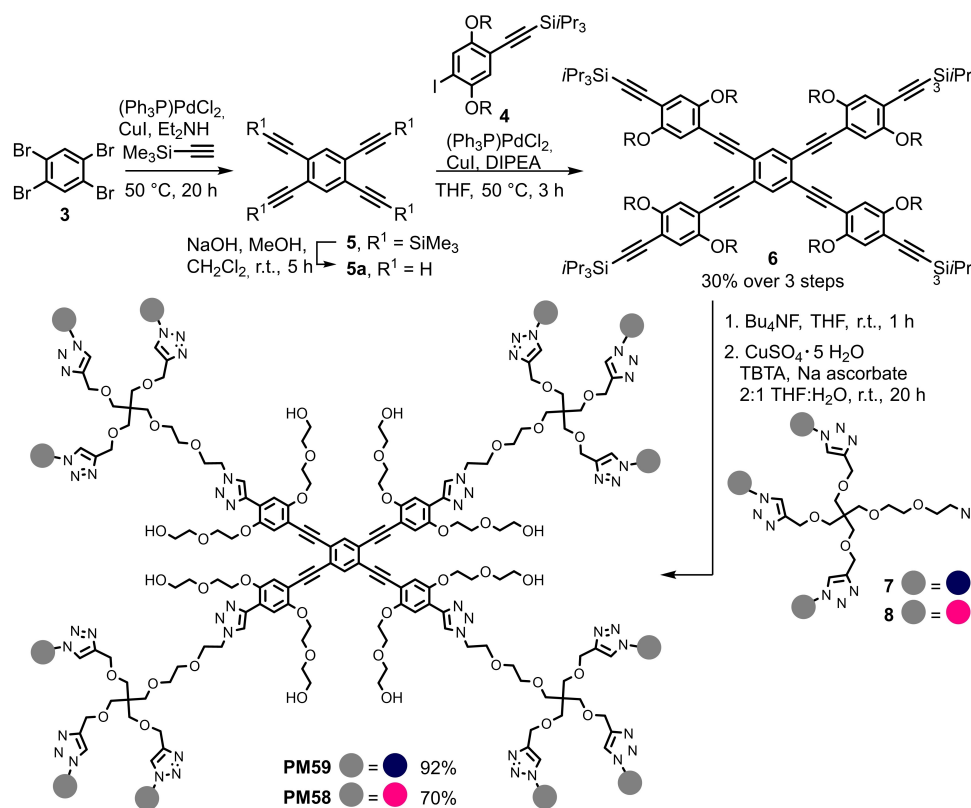
As the first step of the synthesis (Scheme 2), a Sonogashira coupling of 1,2,4,5-tetrabromobenzene **3** with trimethylsilylacetylene afforded the desired protected tetraalkynyl **5** as a pure product, which was directly submitted to a deprotection

reaction. Removal of the trimethylsilyl groups under basic conditions proceeded smoothly, yielding the tetraalkynyl central unit **5a** with no need of further chromatographic purification. The selective formation of both **5** and **5a** was confirmed by ¹H NMR and electron impact (EI) MS analyses. A second Sonogashira coupling enabled connecting the central unit **5a** to four copies of iodide **4**,^[26] finally providing the protected tetravalent scaffold **6**. The formation of the product was monitored exploiting the intrinsic fluorescence of the construct, which allows its detection by TLC analysis (365 nm irradiation), and by ESI-MS analysis. Purification by flash chromatography followed by size-exclusion chromatography (Sephadex LH-20 column) afforded the pure core **6** in 30% yield over three steps from **3**.

With the phenylene-ethynylene core **6** in hand, the glycodendrimers **PM58,59** were finally accessible (Scheme 2). *In situ* deprotection of the terminal alkyne moieties within **6** was accomplished upon treatment with a Bu₄NF solution in THF for 1 h, and monitored by TLC analysis at 365 nm until full conversion was observed. A subsequent CuAAC step guaranteed efficient functionalization of the rigid tetravalent scaffold with four copies of either azido tethered glycodendrimer **7** or **8**.^[21] The reaction progression was assessed either by MALDI-TOF MS (DHB matrix) or HPLC analysis; purification by size-exclusion chromatography (Sephadex LH-20) afforded the final constructs **PM59** and **PM58** in very good yield (92% and 70% respectively). Pleasantly, the constructs showed good solubility in water (**PM59**, 2.5 mM) or water + 4% DMSO solution (**PM58**,



Scheme 1. Retrosynthetic analysis for the preparation of key intermediate **6**.



Scheme 2. Synthetic route towards the cross-shaped glycodendrimers **PM58,59**.

0.2 mM); they were fully characterized by NMR and HRMS analysis and their purity was assessed by HPLC analysis.

Surface plasmon resonance interaction studies: DC-SIGN versus Langerin selectivity

The biological activity of glycodendrimers **PM59** and **PM58** towards DC-SIGN S-ECD and langerin S-ECD was assessed and compared with the corresponding linear constructs **PM31** and **PM26** by an established Surface Plasmon Resonance (SPR) direct interaction assay (Figure 3).^[28]

In this test, increasing concentrations of glycodendrimer solutions are flown over the surface of a sensor chip, functionalized with the immobilized targeted C-type lectins. Analysis of the assay sensorgrams provides the corresponding thermodynamic apparent dissociation constants K_{Dapp} for the direct interaction with Langerin and DC-SIGN surfaces, whose ratio gives the selectivity factor, S (Table 1) of each ligand. The K_{Dapp} values collected in Table 1 refer to the full dendrimer and are not valency corrected.

These tests show that the glycodendrimers **PM58,59** strongly bind to DC-SIGN in comparable way with the previously reported linear **PM31, PM26**.^[18] The **PM59** construct, loaded with 12copies of the pseudo-1,2-mannobioside ligand **1**, is almost twice more effective than its related hexavalent linear glycoconjugate **PM31** ($K_D = 14.4$ nM and 27.3 nM respectively).

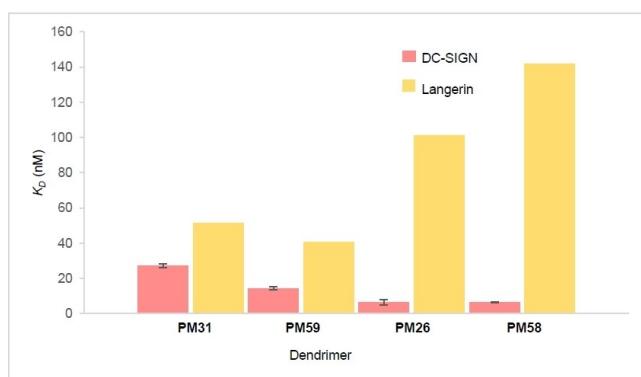


Figure 3. Comparison of dissociation constant K_D values of glycodendrimers **PM31, PM26, PM59** and **PM58** towards DC-SIGN (red bar, number of replicates $n=2$) and langerin (yellow bar, $n=1$) obtained by direct interaction SPR assay. The intrinsic activity of the monovalent ligands **1** and **2**, estimated by binding inhibition assays (SPR) are 0.9 and 0.3 mM, respectively.^[11]

Table 1. Dissociation constants K_{Dapp} (nM) and selectivity factor S of glycodendrimers **PM31, PM26, PM59** and **PM58** obtained for direct interaction with DC-SIGN and Langerin by SPR assays.

Dendrimer	K_{Dapp} (nM)	S	
		DC-SIGN	Langerin
PM31	27.3 ± 1	51.6	1.9
PM59	14.45 ± 0.85	40,6	2.8
PM26	6.6 ± 1.45	101	15
PM58	6.45 ± 0.3	142	22

On the other hand, the constructs carrying the more active and selective bis-amide monovalent ligand **2**, i.e. the cross-shaped **PM58** and linear **PM26** glycodendrimers, exhibit the same potency ($K_D = 6.45$ nM and 6.6 nM respectively), corresponding to a lower multivalency enhancement factor (β) for the higher valency **PM58**. Direct interaction studies with langerin ECD showed that selectivity depends mostly on the nature of the monovalent ligand: both the **PM26** and **PM58** constructs loaded with the intrinsically DC-SIGN selective ligand **2** discriminate effectively against langerin and for DC-SIGN. However, interestingly, the introduction of the tetravalent core within the dendrimer scaffold translates into an increased selectivity towards DC-SIGN, with **PM58** reaching a factor of 22.

Inhibition of DC-SIGN binding to SARS-CoV-2 spike protein

We have recently shown that DC-SIGN binds to immobilized SARS-CoV-2 spike protein and that **PM26** inhibits this binding in an SPR competition experiment.^[20]

The inhibition curves of **PM26, PM58** and **PM59** in the same experiment are compared in Figure 4. These data confirm that the nature of the monovalent spearhead is the main determinant of activity for these ligands, as the cross-shaped ligand **PM58** ($IC_{50} = 5.9 \pm 0.6$ μ M) is about 5 fold more active than **PM59** ($IC_{50} = 26.8 \pm 4$ μ M), but, similar to **PM26** ($IC_{50} = 10.4 \pm 0.4$ μ M), considering that **PM58** has twice the valency of **PM26**. These IC_{50} in the μ M range, as opposed to the nM values of the K_{Dapp} measured above, reflect the context of a competition assay, where the DC-SIGN/Spike protein is now the reporter interaction and where the spike proteins are themselves highly glycosylated.

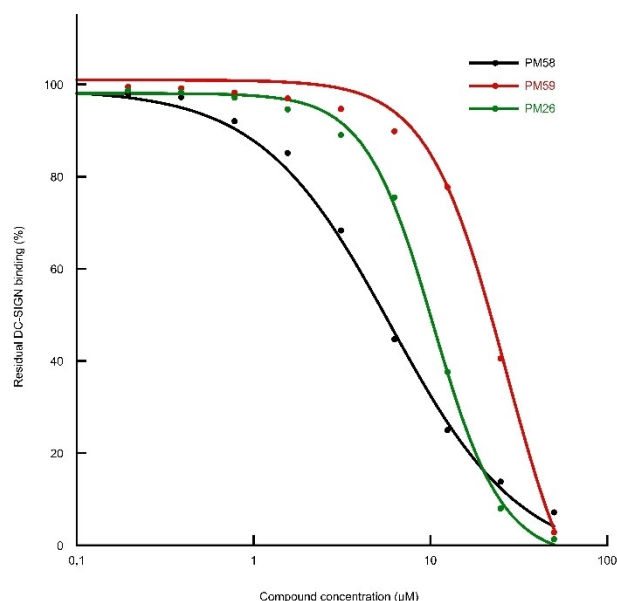


Figure 4. Inhibition curves of DC-SIGN binding to immobilized SARS-CoV-2 Spike protein. Residual DC-SIGN binding was measured by SPR, using **PM26** (green), **PM58** (black) and **PM59** (red).

Inhibition of DC-SIGN mediated trans-infection by Ebola virus

Finally, the antiviral activity of the cross-based systems was tested and compared to **PM26** in a cellular model of Ebola virus infection. The model uses pseudotyped recombinant vesicular stomatitis virus-luciferase (rVSV-luc) viral particles presenting the Ebola envelope glycoprotein (EBOV), and a Jurkat cell line expressing DC-SIGN on the surface, which can transfer the virus to VeroE6 cells (trans-infection).^[29] rVSV-luc particles pseudotyped with VSV glycoprotein were used as a negative control (Supporting information). The results of the infection assay are shown in Figure 5. They are calculated relative to the infection level observed in the absence of inhibitors (negative control), which is assigned 100% value. Both **PM59** and **PM58** at 500 nM block EBOV trans-infection by 88% and 96%, respectively, while **PM26**, at the same concentration is only 63% effective. In this case, it is possible that the increase in activity observed for the cross-shaped systems is related to the ability to cross-link different DC-SIGN tetramers, which, being embedded within the Jurkat cells' membrane rather than immobilized on the SPR sensor surface, retain translational mobility and can cluster in response to binding stimuli.

Discussion

The early involvement of DC-SIGN in the setting of viral infections makes it a promising target in the development of antiadhesive drugs. Most of the antagonists developed so far interact with DC-SIGN by mimicking the highly mannoseylated structure of the naturally occurring (Man)₉(GlcNAc)₂ ligand, commonly referred to as Man₉, which is often exposed in multiple presentation by several pathogenic proteins. Although potent DC-SIGN antagonists have been also obtained by multivalent presentation of the Man₉ oligosaccharide,^[30] a high

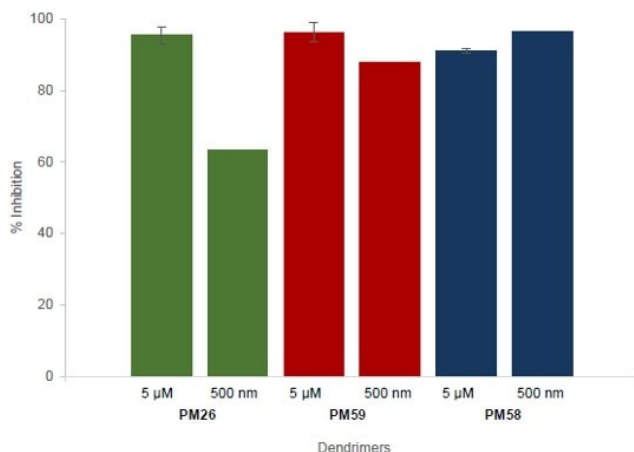


Figure 5. Inhibition of trans-infection of Jurkat DC-SIGN with EBOV-pseudotyped rVSV-luc. Results are presented as percentage of EBOV trans-infection in the presence of compounds: **PM26**, **PM59** and **PM58** as compared to trans-infection of EBOV in VeroE6 mediated by Jurkat DC-SIGN in the absence of inhibitors. EBOV-pseudotyped rVSV-luc was used at MOI: 0.5. The results were analysed using GraphPad Prism v8.

valency of a complex oligosaccharide is typically required to achieve compounds with K_D in the low nanomolar range. The synthesis of such constructs in homogeneous glycosylated form is still a highly demanding and challenging task. Thus, multivalent display of Man₉ mimics is often regarded as a preferred option. Oligomannoside mimics preserve or even improve binding affinity towards DC-SIGN, while presenting a simplified, more synthetically accessible structure, thus allowing the straightforward preparation of potent multivalent antagonists with a relatively low ligand valency.

During the past years, we have disclosed multivalent presentations of glycomimetics as a successful strategy to access potent and selective DC-SIGN antagonists. Our endeavors have led to the pseudo-1,2-dimannobiosides **1,2**, which mimic the Man α (1,2)Man terminal epitopes of Man₉, featuring increased potency, improved drug-like properties and higher stability towards glycosidases. Both mimics have been obtained replacing the reducing end mannose of the Man α (1,2)Man unit by a conformationally locked cyclohexanediol ring, with the bis-amido derivative **2** performing as the most potent and selective of the series.^[11,23] Multivalent presentation of mimics **1,2** with glycodendrimers was crucial to achieve high levels of avidity,^[21] which was boosted when the glycomimetics were loaded on the linear rigid **PM31**, **PM26** dendrimers, specifically tailored to enable chelation of contiguous or opposite CRDs within the DC-SIGN tetramer.^[12,18]

Herein we have presented the structurally related cross-shaped glycodendrimers **PM59** and **PM58**, which are extended enough to simultaneously reach the four CRDs of DC-SIGN. Key for the preparation of the constructs was the synthesis of the four arms intermediate **6**, which was readily accessed by a streamlined route from tetrabromobenzene **3**. The four protected terminal alkynes moieties of **6** allow to functionalize the scaffold in a modular fashion and to obtain **PM59** and **PM58** through a straightforward one-pot deprotection-CuAAC sequence.

The role of the phenylene-ethynylene core of glycodendrimers **PM59** and **PM58**, is of crucial importance. The rigidity and planarity of the structure favor binding by preorganizing the ligands, while decreasing the overall entropy of the system. Of equal importance is the presence of polyethylene glycol chains appended to the core, which impart water solubility to the dendrimers, a fundamental requirement for use in biological settings.

Direct interaction studies with DC-SIGN oriented surfaces performed by SPR assay (Figure 3) revealed that both **PM59** and **PM58** act as potent antagonists, binding DC-SIGN with nanomolar activity ($K_D = 14.4$ nM and 6.4 nM respectively). As expected, higher potency was shown by dendrimer **PM58**, bearing multiple copies of the most performing monovalent bis-amido ligand **2**. However, the increased valency of the cross-shaped **PM59** and **PM58**, is not reflected in a significant gain of avidity, as confirmed by comparing the K_D of these constructs with those of the respective linear constructs **PM31**, **PM26**. This observation suggests that while multivalent effects, comprising chelation of adjacent CRDs, are still operative, simultaneous coordination of the four CRDs of DC-SIGN may

not be occurring, or may not have a significant effect in reducing the dissociation constant of the complex. This is also observed in SPR inhibition studies performed using the spike protein of SARS-CoV-2 as a reporter (Figure 4). Here **PM58** inhibits DC-SIGN binding with an IC_{50} which is ca. half of the value measured for **PM26**, which corresponds to the same potency, considering the valency of the constructs. However, preliminary trans-infection inhibition studies performed in a cellular model (Figure 5) show that that the cross-shaped ligand **PM58** is more effective than **PM26** at blocking DC-SIGN mediated EBOV infection and suggest that the more complex structure may be able to cross-link different DC-SIGN tetramers, which can laterally translate and cluster on the cell membrane.

The selectivity of the dendrimers for DC-SIGN was assessed by SPR direct interaction studies with langerin, a transmembrane C-type lectin also showing affinity for mannosides, but characterized by an homotrimeric structure, with the CRDs exposed in a trefoil presentation with binding sites separated by 4.2 nm.^[31] Selectivity against langerin is an important feature when blocking DC-SIGN in the context of HIV infections, since langerin has a confirmed role in elimination of this virus. The high degree of selectivity observed for **PM58** (Table 1, $S=22$) and **PM26** ($S=15$), bearing the monovalent ligand **2**, is dictated by the selectivity of the latter.^[11] Remarkably, despite the modest contribution to potency, the tetravalent rigid core positively affects the relative selectivity of the dendrimers, which increases by almost two-fold (Table 1 **PM31** vs **PM26** and **PM59** vs **PM58**). This enhancement might possibly arise from the square arrangement of the ligands imparted by the rigid planar core of the dendrimers, which may disfavor binding towards C-type lectins with different topology of the CRDs.

We have shown with **PM26** that the combination of a rigid core with flexible trivalent ligands allows to exploit both chelation and statistical rebinding effects and to achieve high affinity with relatively low valency of the construct.^[12] The merit of this design was also noted in structurally different systems^[32] and has the additional advantage of being able to adapt to the dynamics of oligomeric targets, as well as to the intrinsic mobility of the single recognition domain. More generally, ligands consisting of geometrically matching cores connected by flexible linkers to monovalent ligand units have been demonstrated as a robust, modular and widely applicable design to target multivalent receptors.^[33] The extended core of the glycodendrimers here described allows multivalent display of ligands in a spatially defined fashion at the four corners of a square of 2.2 nm diagonal and should be applicable to a wide array of situations where binding to a tetravalent receptor is sought after.

Conclusion

We were able to study the interaction between DC-SIGN and two glycodendrimer antagonists possessing the structural requirements to simultaneously reach the four CRDs exposed by the target lectin. The novel constructs are characterized by a rigid cross-shaped scaffold, which pre-organizes and directs the

ligands to fit the CRDs arrangement of DC-SIGN, and by the presence of PEG pendants, which confer water solubility to the dendrimers. This central property allowed to evaluate the biological activity of the dendrimers by SPR assays as well as their selectivity over langerin. Moreover, the glycodendrimers were able to inhibit DC-SIGN binding to SARS-CoV-2 spike protein and DC-SIGN mediated trans-infection by Ebola virus. Altogether these studies demonstrated that both **PM59** and **PM58** act as potent antagonists of DC-SIGN. The results suggest that while the constructs are probably able to chelate two adjacent CRDs, a fine tuning for a better compromise between rigidity and flexibility is likely necessary to accomplish a tetracoordination of the tetramer. Importantly, the improved selectivity displayed by the cross-shaped glycodendrimers **PM59** and **PM58**, compared to linear analogs **PM31**, **PM26**, confirms structure-based design as a powerful approach for planning and developing multivalent antagonists with increased DC-SIGN targeting. Finally, straightness and modularity are remarkable characteristics of the synthetic route that we adopted. Analogous elaboration of scaffolds with proper geometry could enable the generation of multivalent antagonists selective for a variety of pattern-recognizing receptors.

Experimental Section

General methods

Chemicals were purchased from commercial sources and used without further purification, unless otherwise indicated. When anhydrous conditions were required, the reactions were performed under nitrogen atmosphere. Anhydrous solvents were purchased from Sigma-Aldrich® with a content of water $\leq 0.005\%$. *N,N'*-Diisopropylethylamine (DIPEA) was dried over calcium hydride, THF was dried over sodium/benzophenone and freshly distilled before use. Reactions were monitored by analytical thin-layer chromatography (TLC) performed on Silica Gel 60 F₂₅₄ plates (Merck) with UV detection (254 nm and 365 nm) and/or staining with ammonium molybdate acid solution or potassium permanganate alkaline solution. Flash column chromatography was performed according to the method of Still and co-workers using silica gel 60 (40–63 μm) (Merck). Size-exclusion chromatography was performed using Sephadex LH-20 from GE Healthcare Life Science. HPLC analyses were performed with an Atlantis T3 5 μm 4.6 \times 100 mm column (Waters) equipped with a Waters 996 Photodiode Array Detector. NMR experiments were recorded either on a Bruker AVANCE-600 MHz or a Bruker AVANCE-400 MHz instrument at 298K. Chemical shifts (δ) are reported in ppm. The ¹H and ¹³C NMR resonances of compounds were assigned with the assistance of COSY and HSQC experiments. Multiplicities are assigned as s (singlet), d (doublet), t (triplet), q (quintet), m (multiplet), b (broad). EI-MS spectra were collected using a VG AUTOSPEC-M246 spectrometer (double-focusing magnetic sector instrument with EBE geometry) equipped with EI source. Solid samples were introduced via a heated direct insertion probe. ESI-MS spectra were recorded on Waters Micromass Q-TOF (ESI ionization-HRMS). MALDI-TOF MS spectra were recorded on Bruker Daltonics Microflex LT. The following abbreviations are used: CuAAC (copper catalyzed azide alkyne cycloaddition), DHB (2,5-dihydroxybenzoic acid), DIPEA (*N,N'*-diisopropylethylamine), HCCA (α -cyano-4-hydroxycinnamic acid), TBTA (tris[(1-benzyl-1*H*-1,2,3-triazol-4-yl)methyl]amine), TFA (trifluoroacetic acid), THF (tetrahydrofuran). Compounds **4**,^[26] **7**,^[21]

and **8**^[21] were previously synthesized in our group. Tetrabromobenzene **3** is commercially available.

Synthetic Procedures

Synthesis of 1,2,4,5-tetrakis(trimethylsilyl)ethynylbenzene **5**^[27]

Tetrabromobenzene **3** (158 mg, 0.40 mmol) was dissolved under nitrogen atmosphere with distilled Et₂NH (2 mL) and (Ph₃P)₂PdCl₂ (7.1 mg, 0.010 mmol), CuI (1.0 mg, 0.005 mmol), ethynyltrimethylsilane (270 μL, 1.92 mmol) were added in the order. The reaction was stirred at 50 °C for 19 h, TLC analysis showed complete conversion (eluent: *n*-hexane, R_f=0.08). The mixture was filtered over a celite pad and washed with Et₂O. Evaporation of the solvent afforded crude **5** that was pure enough to be used in the next synthetic step without further purification. The spectroscopic data are in accordance with those previously reported in the literature. ¹H NMR (400 MHz, CDCl₃) δ (ppm): 7.56 (s, 2 H), 0.25 (s, 36 H). MS (ESI) *m/z*: calcd for C₂₆H₃₈Si₄ 462.20; found 485.08 [M + Na]⁺.

Synthesis of 1,2,4,5-tetraethynylbenzene **5a**^[27]

Crude **5** (50.6 mg, 0.109 mmol) was dissolved under nitrogen atmosphere in dry CH₂Cl₂ (900 μL). Then a NaOH solution in MeOH (45.2 mg in 700 μL) was added and the reaction was stirred at room temperature for 5 h, monitoring by TLC (eluent: *n*-hexane – EtOAc, 20:1, R_f=0.33). The solvent was evaporated, the crude was dissolved in CH₂Cl₂ (5 mL) and filtered washing with fresh CH₂Cl₂ (5 mL) to remove a white precipitate. The organic phase was washed with brine (2×5 mL) and dried over anhydrous Na₂SO₄. Evaporation of the solvent afforded crude **5a** that was pure enough to be used in the next synthetic step without further purification. The spectroscopic data are in accordance with those previously reported in the literature. ¹H NMR (400 MHz, CDCl₃) δ (ppm): 7.64 (s, 2 H), 3.42 (s, 4 H). MS (EI) *m/z*: calcd for C₁₄H₆ 174; found 174 [M]⁺.

Synthesis of compound **6**

Crude **5a** (2.7 mg, 0.012 mmol) was dissolved under nitrogen atmosphere in dry THF (70 μL) and (Ph₃P)₂PdCl₂ (1.3 mg, 0.002 mmol), CuI (1.5 mg, 0.008 mmol), distilled DIPEA (12 μL, 0.069 mmol) were added in the order. Finally, the aryl iodide **4** (40 mg, 0.068) was added as a solution in dry THF (84 μL). The reaction was stirred at 50 °C for 3 h and complete conversion was assessed by TLC analysis (eluent: CH₂Cl₂–MeOH, 9:1, R_f=0.61) monitoring at 365 nm. The solvent was evaporated and the product isolated by flash chromatography (eluent: CH₂Cl₂–MeOH, 20:1 for 6 fractions then CH₂Cl₂–MeOH, 15:1). A further purification was performed by size-exclusion chromatography using a Sephadex LH-20 column (Ø=3 cm, height=50 cm; eluent: MeOH) affording pure **6** (7.4 mg, 30% over three steps from **3**). ¹H NMR (400 MHz, CDCl₃) δ (ppm): 7.77 (s, 2 H), 7.02 (s, 4 H), 7.00 (s, 4 H), 4.18 (t, J=4.6 Hz, 8 H), 3.98 (t, J=4.6 Hz, 8 H), 3.83–3.78 (m, 16 H), 3.72–3.68 (m, 16 H), 3.66–3.61 (m, 16 H), 1.14 (s, 84 H). ¹³C NMR (100 MHz, CDCl₃) δ (ppm): 154.4 (C), 153.6 (C), 134.7 (CH), 125.6 (C), 119.3 (CH), 117.6 (CH), 115.2 (C), 114.3 (C), 102.5 (C), 98.0 (C), 93.2 (C), 92.2 (C), 73.1 (2xCH₂), 70.3 (CH₂), 69.7 (2xCH₂), 69.2 (CH₂), 62.0 (CH₂), 61.9 (CH₂), 18.9 (CH₃), 11.5 (C). MS (ESI) *m/z*: calcd for C₁₁₄H₁₆₆O₂₄Si₄ 2032.09; found 700.3 [M + 3Na]³⁺, 1038.93 [M + 2Na]²⁺, 2054.88 [M + Na]⁺.

MS (MALDI) *m/z*: calcd for C₁₁₄H₁₆₆O₂₄Si₄ 2032.1; found 2056.1 [M + Na]⁺ (matrix DHB).

Synthesis of compound **PM59**

The tetravalent cross-shaped scaffold **6** (5.3 mg, 2.6 μmol) was dissolved in freshly distilled THF (105 μL) under nitrogen atmosphere. Bu₄NF (10 μL) was added as a 1M solution in THF and the reaction was stirred at room temperature for 1 h. Complete deprotection was assessed by TLC analysis (eluent: CH₂Cl₂–MeOH, 9:1, R_f=0.29) monitoring at 365 nm. A solution of TBTA (280 μg, 0.53 μmol) in freshly distilled THF (38 μL) was added, followed by 13 μL of a solution of CuSO₄·5 H₂O (60 μg, 0.24 μmol) and 17 μL of a solution of sodium ascorbate (210 μg, 1.06 μmol) both in degassed H₂O (purged with nitrogen). Finally, dendron **7** (20 mg, 11.4 μmol) was added followed by THF (94 μL) and H₂O (102 μL) to reach a ~2:1 THF/H₂O mixture. The reaction was stirred at room temperature, under nitrogen atmosphere, shielded from light for 15 h. The complete conversion into the desired product was assessed by TLC analysis (eluent: CH₂Cl₂–MeOH, 7:3 + 0.5 H₂O, R_f=0.22) monitoring at 365 nm and by MALDI-TOF MS (matrix DHB, HCCA). The copper scavenger QuadraSil MP was added to the solution which was stirred for 15 min. After filtering, the crude was finally purified by size-exclusion chromatography using a Sephadex LH-20 column (Ø=3 cm, height=50 cm; eluent: MeOH) and monitoring by TLC (eluent: CH₂Cl₂–MeOH, 7:3 + 0.5 H₂O). Dendrimer **PM59** was recovered as a bright yellow oil (20.3 mg, 92%). The purity was confirmed by HPLC analysis of an analytical sample by a Waters Atlantis T3 5 μm 4.6×100mm column, plateau at 90% (H₂O + 0.1% TFA) – 10% (CH₃CN + 0.1% TFA) for 1 min followed by a gradient to 100% (CH₃CN + 0.1% TFA) in 10 min, followed by a plateau for 1 min, flow rate 1 mL/min, λ=254 nm, t_R (product)=7.0 min. [α]_D¹⁶ +28.5 (c=0.49 in MeOH). ¹H NMR (600 MHz, D₂O) δ (ppm): 8.39 (bs, 4 H), 7.94 (s, 12 H), 7.80 (bs, 2 H), 7.73 (bs, 4 H), 7.07 (bs, 4 H), 4.96 (s, 12 H), 4.59 (bs, 32 H), 4.46 (bs, 24 H), 4.28 (bs, 8 H), 4.04–3.91 (m, 52 H), 3.90–3.83 (m, 44 H), 3.81 (dd, J=9.5, 3.1 Hz, 12 H), 3.76–3.72 (m, 20 H), 3.72–3.62 (m, 120 H), 3.62–3.57 (m, 20 H), 3.55 (bs, 8 H), 3.49 (bs, 8 H), 3.38–3.21 (m, 32 H), 2.82 (td, J=12.1, 3.0 Hz, 12 H), 2.46 (td, J=12.1, 2.7 Hz, 12 H), 1.96 (t, J=14.0 Hz, 24 H), 1.73 (t, J=13.2 Hz, 12 H), 1.45 (t, J=13.2 Hz, 12 H). ¹³C NMR (100 MHz, D₂O) δ (ppm): 176.9 (C), 176.6 (C), 153.7 (C), 148.7 (C), 144.4 (C), 141.6 (C), 135.0 (CH), 125.8 (C), 125.6 (CH), 125.0 (CH), 120.9 (C), 117.4 (CH), 112.2 (C), 111.8 (CH), 98.8 (CH), 92.5 (C), 84.8 (C), 74.3 (CH), 73.4 (CH), 72.6 (CH₂), 71.8 (CH₂), 70.9 (2xCH), 70.7 (CH), 70.6 (CH), 69.8 (3xCH₂), 69.4 (CH₂), 68.8 (CH₂), 68.1 (4xCH₂), 66.8 (CH), 66.7 (CH₂), 63.7 (CH₂), 61.0 (CH₂), 60.6 (2xCH₂), 52.6 (2xCH₃), 50.1 (2xCH₂), 44.9 (C), 38.7 (2xCH), 27.2 (CH₂), 26.2 (CH₂). HRMS (ESI) *m/z*: calcd for C₃₆₆H₅₃₄N₄₈O₁₇₆ 8421.44331; found 1426.56540 [M + 6Na]⁶⁺, 1707.28033 [M + 5Na]⁵⁺, 1711.67260 [M – H + 6Na]⁵⁺, 2128.36951 [M + 4Na]⁴⁺, 8421.46951 by deconvolution.

Synthesis of compound **PM58**

The tetravalent cross-shaped scaffold **6** (4.1 mg, 2.0 μmol) was dissolved in freshly distilled THF (80 μL) under nitrogen atmosphere. Bu₄NF (7.7 μL) was added as a 1M solution in THF and the reaction was stirred at room temperature for 1 h. Complete deprotection was assessed by TLC analysis (eluent: CH₂Cl₂–MeOH, 9:1, R_f=0.29) monitoring at 365 nm. A solution of TBTA (215 μg, 0.41 μmol) in freshly distilled THF (29 μL) was added, followed by 10 μL of a solution of CuSO₄·5 H₂O (60 μg, 0.24 μmol) and 13 μL of a solution of sodium ascorbate (210 μg, 1.06 μmol) both in degassed H₂O (purged with nitrogen). Finally, dendron **8** (21 mg, 8.7 μmol) was added followed by THF (72 μL) and H₂O (78 μL) to reach a ~2:1 THF/H₂O mixture. The reaction was stirred at room temperature, under nitrogen atmosphere, shielded from light for 5 days. The complete conversion into the desired product was assessed HPLC analysis. The copper scavenger QuadraSil MP was added to the solution which was stirred for 15 min. After filtering,

the crude was finally purified by size-exclusion chromatography using a Sephadex LH-20 column ($\varnothing=3$ cm, height = 50 cm; eluent: MeOH) and monitoring by TLC (eluent: CH_2Cl_2 -MeOH, 7:3 + 0.5 H_2O). Dendrimer **PM58** was recovered as a bright yellow oil (15 mg, 70%). The purity was confirmed by HPLC analysis of an analytical sample by a Waters Atlantis T3 5 μm 4.6 \times 100 mm column, plateau at 90% ($\text{H}_2\text{O} + 0.1\%$ TFA) – 10% ($\text{CH}_3\text{CN} + 0.1\%$ TFA) for 1 min followed by a gradient to 100% ($\text{CH}_3\text{CN} + 0.1\%$ TFA) in 15 min, followed by a plateau for 2 min, flow rate 1 mL/min, $\lambda=254$ nm, t_{R} (product) = 8.0 min. ^1H NMR (600 MHz, $(\text{CD}_3)_2\text{SO}$) δ (ppm): 8.49 (bs, 4 H), 8.30 (bt, $J=5.6$ Hz, 12 H), 8.21 (bt, $J=5.6$ Hz, 12 H), 8.02 (s, 12 H), 7.88 (bs, 4 H), 7.81 (bs, 2 H), 7.26 (bs, 4 H), 7.20 (d, $J=7.1$ Hz, 48 H), 7.14 (t, $J=7.8$ Hz, 48 H), 5.09 (t, $J=5.6$ Hz, 24 H), 4.76 (s, 12 H), 4.73 (d, $J=2.4$ Hz, 12 H), 4.67 (d, $J=2.0$ Hz, 12 H), 4.58 (d, $J=2.7$ Hz, 12 H), 4.55–4.47 (m, 44 H), 4.47–4.40 (m, 72 H), 4.23–4.11 (m, 56 H), 4.11–4.02 (m, 8 H), 3.94–3.86 (m, 8 H), 3.87–3.78 (m, 16 H), 3.78–3.68 (m, 52 H), 3.61 (bs, 12 H), 3.56–3.34 (m, 136 H), 3.17 (d, $J=4.3$ Hz, 8 H), 2.74 (quint., $J=12.6$ Hz, 24 H), 1.83–1.64 (m, 36 H), 1.59 (t, $J=12.2$ Hz, 12 H). ^{13}C NMR (150 MHz, $(\text{CD}_3)_2\text{SO}$) δ (ppm): 174.0 (2x C), 153.7 (C), 148.5 (C), 144.0 (C), 141.0 (C), 140.6 (C), 138.0 (C), 134.4 (CH), 126.6 (2xCH), 126.2 (2xCH), 124.8 (C), 124.7 (CH), 124.1 (CH), 121.9 (C), 117.1 (CH), 111.4 (CH), 111.2 (C), 98.7 (CH), 91.1 (C), 85.5 (C), 74.6 (CH), 74.2 (CH), 72.6 (CH_2), 72.1 (CH_2), 70.9 (CH), 70.5 (CH), 70.4 (CH), 69.3 (CH_2), 69.1 (2x CH_2), 68.8 (2x CH_2), 68.6 (2x CH_2), 67.8 (2x CH_2), 67.0 (CH), 66.5 (CH_2), 64.0 (CH_2), 62.6 (CH_2), 61.3 (CH_2), 60.2 (2x CH_2), 49.3 (2x CH_2), 44.9 (C), 41.5 (2x CH_2), 39.5 (2xCH), 28.2 (CH_2), 27.8 (CH_2). HRMS (ESI) m/z : calcd for $\text{C}_{534}\text{H}_{702}\text{N}_{72}\text{O}_{176}$ 10944.83778; found 1847.13142 [$\text{M} + 6\text{Na}$] $^{6+}$, 2211.96258 [$\text{M} + 5\text{Na}$] $^{5+}$, 10944.85366 by deconvolution.

Surface Plasmon Resonance analysis

All the direct interaction experiments were executed on a T200 Biacore with a CM3 series S sensor chip. DC-SIGN and langerin extracellular domains harboured a StreptagII in their N-terminus (DC-SIGN S-ECD and langerin S-ECD) to allow their capture and functionalization onto the surface in an oriented manner. Flow cells were functionalized as previously described.^[28] Briefly, after EDC/NHS activation, flow cells were functionalized with streptactin protein in a first step. Flow cell 1 was used as it is as control, while other flow cells were, after a second round of activation, functionalized with 49 $\mu\text{g}/\text{mL}$ and 55.9 $\mu\text{g}/\text{mL}$ of DC-SIGN S-ECD and langerin S-ECD, respectively, up to a final density ranging between 2000 and 3000 RU, via tag specific capture and linkage by amine coupling chemistry simultaneously. The compounds were injected in running buffer of 25 mM Tris pH8, 150 mM NaCl, 4 mM CaCl_2 , 0.05% Tween 20 onto the surface at increasing concentrations with a flow rate of 30 $\mu\text{L}/\text{min}$. The ligand titration led to the determination of an apparent K_{D} value. The data was analysed in Biacore BIAevaluation software for steady state affinity calculations assuming that the K_{D} will reflect the affinity of the ligands (glycoclusters) with the DC-SIGN oriented surface.

Inhibition of DC-SIGN binding to SARS-CoV-2 spike protein

Inhibition experiments on the SAR-CoV-2 spike surface were performed as previously described.^[20]

Production of EBOV-pseudotyped rVSV-luc and inhibition assays

Inhibition property of **PM26**, **PM58** and **PM59** was tested by using an EBOV-pseudotyped recombinant vesicular stomatitis virus-luciferase (rVSV-luc) system. rVSV-luc was produced following previously published protocols.^[34] The expression vector encoding

EBOV glycoprotein (strain Makona, GenBank accession no. KM233102.1) was synthesized and cloned into pcDNA3.1 by GeneArt technology (Thermo Fisher Scientific). Pseudotyped viruses were normalized for infectivity to a multiplicity of infection of 0.5 and the inhibitory effect of the glycomimetic compounds: **PM26**, **PM58**, **PM59** was evaluated on DC-SIGN-mediated trans-infection by Jurkat DC-SIGN to susceptible Vero E6 cells.^[29] Jurkat DC-SIGN cells were first pre-incubated 20 min with the corresponding concentration of the compounds before being challenged with EBOV-rVSV-luc. **PM26**, **PM58** and **PM59** were tested at 2 different concentrations: 5 μM and 500 nM. Cells were then incubated with the EBOV-rVSV-luc during 2 h at room temperature with rotation. Cells were then centrifuged at 1200 rpm for 5 minutes and washed with PBS supplemented with 0.5% BSA and 1 mM CaCl_2 three times. Cells were then resuspended in RPMI medium and co-cultivate with adherent VeroE6 cells. After 24 h, the supernatant was removed and monolayer of VeroE6 was washed with PBS three times. Cells were then lysed and assayed for luciferase expression (Glomax Navigator, Promega).

Acknowledgements

This work was supported by a doctoral fellowship from MIUR (G.G.), by a Marie Curie Outgoing Fellowship (C.C.) under REA grant agreement no. PIOF-GA-2012-327579 and by the European Union's Horizon 2020 research and innovation program under the Marie Skłodowska-Curie grant agreement No. 642870 (Immunoshape) (S.A.). Research in RD lab is supported by grants from the Instituto de Investigación Carlos III, ISCIII, (FIS PI21/00989), by the European Commission Horizon 2020 Framework Programme: Project VIRUSCAN FETPROACT-2016: 731868, Horizon Europe Framework Programme: Project EPIC-CROWN-2 Ref.101046084 and by Fundación Caixa-Health Research (Project StopEbola HR18-00469). The UNITECH – COSPECT platform at the University of Milan was used for MS analysis. The Multistep Protein Purification Platform (MP3) was used for human DC-SIGN and langerin S-ECD production and the SPR platform for the direct interaction tests of the Grenoble Instruct center (ISBG; UMS 3518 CNRS-CEA-UJF-EMBL) with support from FRISBI (ANR-10-INSB-05-02) and GRAL (ANR-10-LABX-49-01) within the Grenoble Partnership for Structural Biology. We thank Gabriele Conti for technical help with the synthesis of intermediate 6. Open Access funding provided by Università degli Studi di Milano within the CRUI-CARE Agreement.

Conflict of Interest

The authors declare no conflict of interest.

Data Availability Statement

The data that support the findings of this study are available in the supplementary material of this article.

Keywords: Carbohydrates · DC-SIGN · Dendrimers · Glycomimetics · Langerin

- [1] C. R. Bertozzi, L. L. Kiessling, *Science* **2011**, *291*, 2357–2364.
- [2] M. Mammen, S.-K. Choi, G. M. Whitesides, *Angew. Chem. Int. Ed.* **1998**, *37*, 2754–2794; *Angew. Chem.* **1998**, *110*, 2908–2953.
- [3] C. Fasting, C. A. Schalley, M. Weber, O. Seitz, S. Hecht, B. Kokschi, J. Dervede, C. Graf, E.-W. Knapp, R. Haag, *Angew. Chem. Int. Ed.* **2012**, *51*, 10472–10498; *Angew. Chem.* **2012**, *124*, 10622–10650.
- [4] R. J. Pieters, *Org. Biomol. Chem.* **2009**, *7*, 2013–2025.
- [5] J. E. Hudak, C. R. Bertozzi, *Chem. Biol.* **2014**, *21*, 16–37.
- [6] J. L. Jiménez Blanco, C. Ortiz Mellela, J. M. García Fernández, *Chem. Soc. Rev.* **2013**, *42*, 4518–4531.
- [7] A. Bernardi, J. Jiménez-Barbero, A. Casnati, C. DeCastro, T. Darbre, F. Fieschi, J. Finne, H. Funken, K.-E. Jaeger, M. Lahmann, T. K. Lindhorst, M. Marradi, P. Messner, A. Molinaro, P. V. Murphy, C. Nativi, S. Oscarson, S. Penadés, F. Peri, R. J. Pieters, O. Renaudet, J.-L. Reymond, B. Richichi, J. Rojo, F. Sansone, C. Schäffer, W. B. Turnbull, T. Velasco-Torrijos, S. Vidal, S. Vincent, T. Wennekes, H. Zuilhof, A. Imberty, *Chem. Soc. Rev.* **2013**, *42*, 4709–4727.
- [8] S. Cecioni, A. Imberty, S. Vidal, *Chem. Rev.* **2015**, *115*, 525–561.
- [9] S. Sattin, A. Bernardi, *Trends Biotechnol.* **2016**, *34*, 483–495.
- [10] S. Liese, R. R. Netz, *ACS Nano* **2018**, *12*, 4140–4147.
- [11] N. Varga, I. Sutkevičiūtė, C. Guzzi, J. McGeagh, I. Petit-Haertlein, S. Gugliotta, J. Weiser, J. Angulo, F. Fieschi, A. Bernardi, *Chem. Eur. J.* **2013**, *19*, 4786–4797.
- [12] S. Ordanini, N. Varga, V. Porkolab, M. Thépaut, L. Belvisi, A. Bertaglia, A. Palmioli, A. Berzi, D. Trabattoni, M. Clerici, F. Fieschi, A. Bernardi, *Chem. Commun.* **2015**, *51*, 3816–3819.
- [13] S. Ordanini, G. Goti, A. Bernardi, *Can. J. Chem.* **2017**, *95*, 881–890.
- [14] V. Porkolab, E. Chabrol, N. Varga, S. Ordanini, I. Sutkevičiūtė, M. Thépaut, M. J. García-Jiménez, E. Girard, P. M. Nieto, A. Bernardi, F. Fieschi, *ACS Chem. Biol.* **2018**, *13*, 600–608.
- [15] T. B. H. Geijtenbeek, D. S. Kwon, R. Torensma, S. J. van Vliet, G. C. F. van Duijnhoven, J. Middel, I. L. M. H. A. Cornelissen, H. S. L. M. Nottet, V. N. Kewal Ramani, D. R. Littman, C. G. Figdor, Y. vanKooyk, *Cell* **2000**, *100*, 587–597.
- [16] Y. vanKooyk, A. Engering, A. N. Lekkerkerker, I. S. Ludwig, T. B. H. Geijtenbeek, *Curr. Opin. Immunol.* **2004**, *16*, 488–493.
- [17] S. Ordanini, G. Zanchetta, V. Porkolab, C. Ebel, F. Fieschi, I. Guzzetti, D. Potenza, A. Palmioli, Č. Podlipnik, D. Meroni, A. Bernardi, *Macromol. Biosci.* **2016**, *16*, 896–905.
- [18] V. Porkolab, M. Lepšák, S. Ordanini, A. StJohn, A. LeRoy, M. Thépaut, E. Paci, C. Ebel, A. Bernardi, F. Fieschi, **2022**, DOI 10.26434/chemrxiv-2022-4n79q.
- [19] A. Berzi, S. Ordanini, B. Joosten, D. Trabattoni, A. Cambi, A. Bernardi, M. Clerici, *Sci. Rep.* **2016**, *6*, 35373.
- [20] M. Thépaut, J. Luczkowiak, C. Vivès, N. Labiod, I. Bally, F. Lasala, Y. Grimoire, D. Fenel, S. Sattin, N. Thielens, G. Schoehn, A. Bernardi, R. Delgado, F. Fieschi, *PLoS Pathog.* **2021**, *17*, e1009576.
- [21] N. Varga, I. Sutkevičiūtė, R. Ribeiro-Viana, A. Berzi, R. Ramdasi, A. Daggetti, G. Vettoretti, A. Amara, M. Clerici, J. Rojo, F. Fieschi, A. Bernardi, *Biomaterials* **2014**, *35*, 4175–4184.
- [22] G. Tabarani, M. Thépaut, D. Stroebel, C. Ebel, C. Vivès, P. Vachette, D. Durand, F. Fieschi, *J. Biol. Chem.* **2009**, *284*, 21229–21240.
- [23] J. J. Reina, S. Sattin, D. Invernizzi, S. Mari, L. Martínez-Prats, G. Tabarani, F. Fieschi, R. Delgado, P. M. Nieto, J. Rojo, A. Bernardi, *ChemMedChem* **2007**, *2*, 1030–1036.
- [24] a) H.-C. Wen, C.-H. Lin, J.-S. Huang, C.-L. Tsai, T.-F. Chena, S.-K. Wang, *Chem. Commun.* **2019**, *55*, 9124–9127; b) K. Neuhaus, E.-C. Wamhoff, T. Freichel, A. Grafmüller, C. Rademacher, L. Hartmann, *Biomacromolecules* **2019**, *20*, 4088–4095.
- [25] L. deWitte, A. Nabatov, M. Pion, D. Fluitsma, M. A. W. P. de Jong, T. de Grujil, V. Piguët, Y. van Kooyk, T. B. H. Geijtenbeek, *Nat. Med.* **2007**, *13*, 367–371.
- [26] F. Peticci, N. Varga, A. van Duijn, M. Rey-Carrizo, A. Bernardi, R. J. Pieters, *Beilstein J. Org. Chem.* **2013**, *9*, 215–222.
- [27] C.-C. Wang, H. Tsai, H.-H. Shih, S. Jeon, Z. Xu, D. Williams, S. Iyer, T. C. Sanchez, L. Wang, M. Cotlet, H.-L. Wang, *ACS Appl. Mater. Interfaces* **2010**, *2*, 738–747.
- [28] V. Porkolab, C. Pifferi, I. Sutkevičiūtė, S. Ordanini, M. Taouai, M. Thépaut, C. Vivès, M. Benazza, A. Bernardi, O. Renaudet, F. Fieschi, *Org. Biomol. Chem.* **2020**, *18*, 4763–4772.
- [29] J. Luczkowiak, S. Sattin, I. Sutkevičiūtė, J. J. Reina, M. Sanchez-Navarro, M. Thépaut, L. Martínez-Prats, A. Daggetti, F. Fieschi, R. Delgado, A. Bernardi, J. RojoBioconj, *Chem.* **2011**, *22*, 1354–1365.
- [30] S.-K. Wang, P.-H. Liang, R. D. Astronomo, T.-L. Hsu, S.-L. Hsieh, D. R. Burton, C.-H. Wong, *Proc. Natl. Acad. Sci. USA* **2008**, *105*, 3690–3695.
- [31] H. Feinberg, A. S. Powlesland, M. E. Taylor, W. I. Weis, *J. Biol. Chem.* **2010**, *285*, 13285–13293.
- [32] G. Bachem, E.-C. Wamhoff, K. Silberreis, D. Kim, H. Baukman, F. Fuchsberger, J. Dervede, C. Rademacher, O. Seitz, *Angew. Chem. Int. Ed.* **2020**, *59*, 21016–21022; *Angew. Chem.* **2020**, *132*, 21202–21208.
- [33] S. Liese, R. R. Netz, *ACS Nano* **2018**, *12*, 4140–4147.
- [34] a) M. A. Whitt, *J. Virol. Methods* **2010**, *169*, 365–374; b) J. Luczkowiak, N. Labiod, G. Rivas, M. Rolo, F. Lasala, J. Lora-Tamayo, M. Mancheno-Losa, D. Rial, A. Pérez-Rivilla, M. D. Folgueira, R. Delgado, *Open Forum Infect. Dis.* **2021**, *8*, ofab468.

Manuscript received: February 2, 2022
Revised manuscript received: April 28, 2022
Accepted manuscript online: April 29, 2022